JOURNAL OF SOLID STATE CHEMISTRY 6, 574–582 (1973)

Crystal Structures and Magnetic Structures of Some Metal(I) Chromium(III) Sulfides and Selenides

F. M. R. ENGELSMAN, G. A. WIEGERS, F. JELLINEK

Laboratorium voor Anorganische Chemie, Rijksuniversiteit, Zernikelaan, Groningen, The Netherlands

AND

B. VAN LAAR

Reactor Centrum Nederland, Petten (N.H.), The Netherlands

Received July 18, 1972

The crystal structures of the rhombohedral compounds $ACrX_2$ (A = Na, Ag, Cu; X = S, Se) at 300 and 4 K have been refined from neutron-diffraction powder data. The structures are based on cubic close-packings of the anions with Cr in half of the octahedral holes, so that CrX_2 sandwiches are formed. Na occupies the octahedral holes between these sandwiches, Ag and Cu half of the tetrahedral holes; Ag and Cu have anomalously large (and anisotropic) thermal parameters, probably indicating a statistical distribution of these atoms around their average positions. The Ag and Cu compounds undergo reversible phase transitions at 397°C ($AgCrS_2$), 402°C ($CuCrS_2$), or 202°C ($AgCrSe_2$); in the high-temperature forms the Ag and Cu atoms are randomly distributed over all tetrahedral holes between the CrX_2 sandwiches.

The magnetic structures of $NaCrS_2$, $NaCrSe_2$, and $AgCrSe_2$ at 4.2 K have been determined by neutron diffraction. The magnetic moments of Cr^{3+} (about 15% less than the spin-only value) are perpendicular to the c axis. The moments in pseudohexagonal (110) planes are collinear, spins at a distance $(-\frac{1}{3}, \frac{1}{3}, \frac{1}{3})$ being antiparallel, spins at a distance $(\frac{1}{3}, -\frac{1}{3}, \frac{2}{3})$ parallel. The spins in adjacent (110) planes make angles φ, where $\varphi = 0°$ for $NaCrSe_2$, $\varphi = 14°$ for $AgCrSe_2$, $\varphi = 33°$ for $NaCrS_2$. Thus, $NaCrSe_2$ consists of ferromagnetic layers perpendicular to c, the spins in adjacent layers being antiparallel. In $NaCrS_2$ and $AgCrSe_2$ the layers are helimagnetic. These magnetic structures and those of $KCrS_2$ and $LiCrS_2$ are discussed in terms of antiferromagnetic direct Cr–Cr interactions and ferromagnetic Cr–X–Cr interactions between Cr neighbors in the layers; the former interaction predominates for small, the latter for large Cr–Cr distances.

1. Introduction

The crystal structures at room temperature of $NaCrS_2$, $CuCrS_2$, $AgCrS_2$, and of the corresponding selenides have been reported by Bongers et al. (*1*). The structures of these rhombohedral compounds are based on a somewhat distorted cubic close-packing of the anions. The Cr^{3+} ions occupy octahedral holes so that CrX_2^- sandwiches are formed (X = S, Se). Between these sandwiches, the monovalent cations are situated, Na^+ in octahedral holes (space group $R\bar{3}m$), Cu^+ and Ag^+ in half of the tetrahedral holes (space group $R3m$); see Fig. 1a, b.

The magnetic properties of the same compounds (except $CuCrSe_2$) were also studied by Bongers et al. (*1*); they are summarized in Table I. All compounds become antiferromagnetic at low temperatures. $NaCrSe_2$, $AgCrSe_2$, and $NaCrS_2$ have positive asymptotic Curie temperatures Θ. This indicates that the dominating intralayer interaction between the Cr^{3+} ions is positive; it seemed plausible that the magnetic structure of these compounds below the Néel temperature T_N consists of ferromagnetic layers that are antiferromagnetically coupled. Large deviations from the Curie–Weiss law are observed above T_N up to about $T = 2\Theta$, indicating a large amount of short-range magnetic order within the layers. The results of low-temperature measurements on stacks of single-crystal platelets

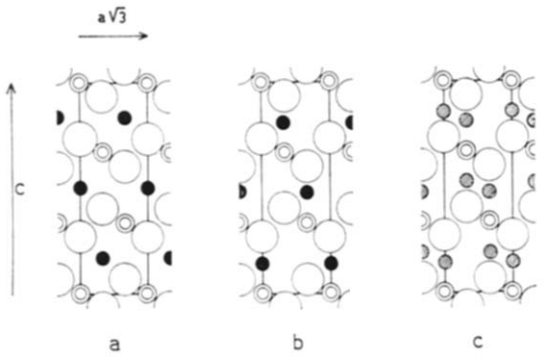

FIG. 1. Sections through the (11$\bar{2}$0) planes of: (a) $NaCrX_2$ (X = S, Se); (b) Low-temperature form of $CuCrX_2$ and $AgCrX_2$; (c) High-temperature form of $CuCrS_2$ and $AgCrX_2$. Large open circles indicate chalcogen atoms, double circles Cr atoms; fully occupied positions of Na, Cu, Ag are shown as black circles, statistically occupied positions as hatched circles.

of $NaCrS_2$ were said to be consistent with a helical arrangement of the spins (*1*).

The magnetic susceptibilities of $CuCrS_2$ and $AgCrS_2$ follow the Curie–Weiss law more closely down to the Néel temperature which appears as a sharp kink in the $\chi^{-1}(T)$ curve. These compounds have negative values of Θ, indicating that ferromagnetic layers of Cr^{3+} (as in the selenides) are not present below T_N.

The present communication reports refinements of the crystal structures of $NaCrS_2$, $CuCrS_2$, $AgCrS_2$, $NaCrSe_2$, and $AgCrSe_2$ at room temperature, a study of phase transitions observed in the Cu and Ag compounds at elevated temperatures, and the determination of the magnetic structures of $NaCrS_2$, $NaCrSe_2$, and $AgCrSe_2$ at 4 K. Most of our results are based on neutron-diffraction data from polycrystalline samples.

TABLE I

ASYMPTOTIC CURIE TEMPERATURE Θ AND NÉEL TEMPERATURE T_N OF THE COMPOUNDS $ACrX_2$[a]

	Θ (K)	T_N (K)	C_M[b]	q
$NaCrS_2$	+30	19	1.79	2.91
$CuCrS_2$	−90	39	1.78	2.90
$AgCrS_2$	−55	40	1.71	2.83
$NaCrSe_2$	+108	40	1.84	2.96
$AgCrSe_2$	+72	50	1.70	2.82

[a] A = Na, Cu, Ag; X = S, Se.

[b] The molar Curie constant C_M in the paramagnetic range and the deduced number of unpaired electrons (q) are also given.

2. Experimental

The compounds studied were prepared as described previously (*1*), their purity was checked by X-ray diffraction. High-temperature X-ray powder patterns were taken with a Guinier–Lenné camera (Nonius); the temperature was varied continuously between 290 and about 900 K. Powder patterns in the range 100–300 K were taken with a similar camera which had been adapted for working at low temperatures (*2*). Differential thermal analyses in the range 90–800 K were performed with apparatus constructed by J. C. Wildervanck and J. Koopstra. Neutron-diffraction data up to $\sin\Theta/\lambda = 0.37$ Å^{-1} at 300 K and 4.2 K (for $AgCrSe_2$ also at 525 K) were collected on the powder diffractometer at the H.F.R. in Petten. A neutron wavelength of 2.57 Å was obtained from the (111) plane of a copper crystal. As a second-order filter, a block of pyrolytic graphite with a thickness of 10 cm, was employed (*3*). Between reactor and monochromator and in front of the BF_3 counter Soller slits with a horizontal angular divergence of 30′ were placed. The samples were contained in cylindrical vanadium sample holders with diameters of 15 or 20 mm.

For the refinement of the structural and the magnetic parameters from neutron diffractograms the line-profile method described by Rietveld (*4*) was applied. For the magnetic form factor of Cr, the one given by Watson and Freeman (*5*) for Cr^{3+} was used.

3. Structures at Room Temperature (300 K)

The crystal structures of $NaCrS_2$ (*6*, *7*) and $NaCrSe_2$ (*8*) reported previously were confirmed. These compounds crystallize in space group $R\bar{3}m - (D_{3d}^5)$ with the following atomic positions, referred to hexagonal axes:

3Cr in 3(*a*): 000
3Na in 3(*b*): $00\frac{1}{2}$
6S, Se in 6(*c*): $\pm(00z)$

Refinement by the line-profile method yielded the unit-cell dimensions, atomic parameters, and (isotropic) overall temperature factors given in Tables II, III, and IV. The structures are shown in Fig. 1a.

TABLE II

UNIT-CELL DIMENSIONS OF $ACrX_2$[a]

	T(K)	a(Å)	c(Å)	c/a	U(Å^3)
$NaCrS_2$	4.2	3.5561(7)	19.365(9)	5.446(3)	212.1
	300	3.5544(2)	19.492(1)	5.484(1)	213.3
$CuCrS_2$	4.2	3.4728(7)	18.616(3)	5.361(3)	194.4
	300	3.4812(4)	18.697(1)	5.370(2)	196.3
$AgCrS_2$	4.2	3.4884(9)	20.414(4)	5.852(3)	215.1
	300	3.4974(4)	20.481(2)	5.856(2)	217.0
$NaCrSe_2$	4.2	3.7323(3)	20.237(4)	5.422(2)	244.1
	300	3.7323(2)	20.396(3)	5.465(2)	246.1
$AgCrSe_2$	4.2	3.6898(9)	21.024(6)	5.698(3)	247.9
	300	3.6809(8)	21.210(6)	5.762(3)	248.9
	525	3.6821(3)	21.231(2)	5.766(2)	249.3

[a] A = Na, Cu, Ag; X = S, Se; standard deviations in units of the last decimal place are given in parentheses.

$CuCrS_2$, $AgCrS_2$, and $AgCrSe_2$ crystallize in space group $R3m-(C_{3v}^5)$ with all atoms in position 3(*a*): $00z$; $\frac{2}{3},\frac{1}{3},\frac{1}{3}+z$; $\frac{1}{3},\frac{2}{3},\frac{2}{3}+z$ (1) (Fig. 1b). Refinement of the structures of $AgCrS_2$ and $AgCrSe_2$ with overall isotropic temperature factors did not lead to satisfactory intensity agreement, considering the accuracy of the experimental intensities. Analysis revealed the apparent thermal motion of the Ag atoms to be much larger than that of the other atoms and strongly anisotropic, the root-mean-square (rms) deviation from the *c* axis being very large (Table IV). Probably, the apparent thermal motion should be interpreted as a statistical distribution of Ag over several positions in the tetrahedral holes, corresponding to an rms deviation $\mu_a=\mu_b=0.28$ Å from the trigonal axis and an rms deviation of 0.17 Å in the *c* direction, both for $AgCrS_2$ and $AgCrSe_2$.

In $CuCrS_2$ the apparent thermal motion of Cu is again larger than that of the other atoms, but the anisotropy is not pronounced (Table IV). The thermal parameters of Cu correspond to an rms deviation $\mu_a=\mu_b=0.17$ Å, and an rms deviation of 0.19 Å in the *c* direction. The atomic parameters of Cr, S, Se and of the average positions of Ag and Cu are given in Table III, the unit-cell dimensions in Table II; the agreement with previous—less accurate—values (*1*) is satisfactory.

TABLE III

ATOMIC PARAMETERS IN $ACrX_2$[a]

	T(K)	Space group[b]	z(A)	z(X1)	z(X2)
$NaCrS_2$	4.2	*c*	0.5(—)	0.2667(6)[c]	
	300	*c*	0.5(—)	0.2662(4)	
$NaCrSe_2$	4.2	*c*	0.5(—)	0.2655(2)	
	300	*c*	0.5(—)	0.2656(1)	
$CuCrS_2$	4.2	*a*	0.1475(4)	0.2661(6)	0.7417(7)
	300	*a*	0.1481(3)	0.2657(4)	0.7425(5)
$AgCrS_2$	4.2	*a*	0.1527(5)	0.2703(8)	0.7324(7)
	300	*a*	0.1560(3)	0.2713(5)	0.7341(5)
$AgCrSe_2$	4.2	*a*	0.1518(9)	0.2694(9)	0.7335(9)
	300	*a*	0.1529(8)	0.2694(8)	0.7335(7)
	525	*c*	0.1525(4)	0.2679(1)	

[a] A = Na, Cu, Ag; X = S, Se; $z(\mathrm{Cr})\equiv 0$ in all cases.
[b] $a=R3m-C_{3v}^5$; $c=R\bar{3}m-D_{3d}^5$.
[c] Standard deviations in units of the last decimal place are given in parentheses.

TABLE IV

ROOT-MEAN-SQUARE DISPLACEMENTS FROM AVERAGE ATOMIC POSITIONS[a]

		Cu or Ag		Na, Cr, S, Se
	T(K)	μ_a(Å)	μ_c(Å)	$\mu_a=\mu_c$(Å)
$NaCrS_2$	4.2			0.09(1)
	300			0.13(1)
$NaCrSe_2$	4.2			—
	300			0.07(1)
$CuCrS_2$	4.2	0.1		—
	300	0.17(1)	0.19(1)	—
$AgCrS_2$	4.2	0.1		—
	300	0.28(1)	0.17(2)	0.05(1)
$AgCrSe_2$	4.2	0.2		—
	300	0.28(1)	0.17(2)	—
	525	0.50(1)	0.19(2)	0.07(1)

[a] Standard deviations in units of the last decimal place are given in parentheses. A bar (—) indicates that the root-mean-square displacement is not significantly different from zero.

4. Phase Transitions

The thermal behavior of the compounds under investigation in the range 100–900 K was studied

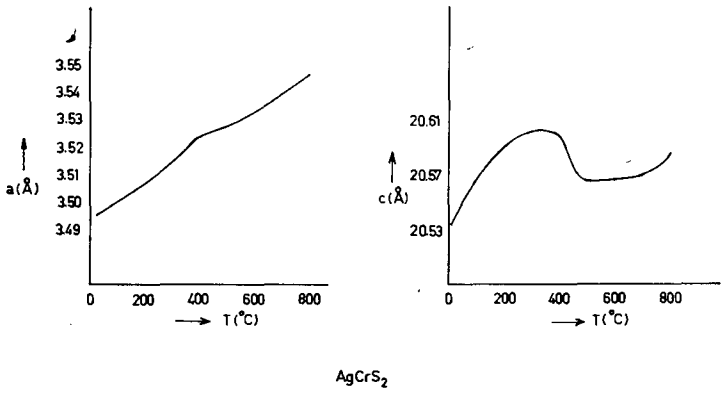

FIG. 2. Unit-cell dimensions of $AgCrS_2$ determined from a high-temperature Guinier diagram.

by differential thermal analysis and X-ray diffraction. Reversible phase transitions were found to occur in $CuCrS_2$ (675 K), $AgCrS_2$ (670 K), and $AgCrSe_2$ (475 K). The D.T.A. curves indicate the transitions to be (close to) second order. High-temperature Guinier photographs did not show discontinuous changes of the unit-cell dimensions at the transition temperatures (Fig. 2), but the intensities of some diffraction lines changed drastically.

Analysis of the intensities showed that the space group of the high-temperature modification is $R\bar{3}m - D_{3d}^5$; the Cu^+ and Ag^+ ions are now statistically distributed over all tetrahedral holes between the CrX_2^- slabs [position 6(*c*)] (Fig. 1c).

The structure of the high-temperature form of $AgCrSe_2$ was refined from neutron-diffraction data obtained at 525 K. Again, the apparent thermal motion of Ag was found to be strongly anisotropic (Table IV and Fig. 3). As before, we ascribe this effect to a statistical distribution of Ag over several positions within each tetrahedral hole. The thermal parameters correspond to an rms deviation $\mu_a = 0.50$ Å and an rms deviation $\mu_c = 0.19$ Å. The positional parameters are included in Table III.

5. Magnetic Structures at 4.2 K

$NaCrSe_2$

The neutron-diffraction diagram of $NaCrSe_2$ at 4.2 K showed a number of clear magnetic reflections which could be indexed on the basis of a hexagonal unit cell with edges $a' = a$ and $c' = 2c$; a and c are the edges of the nuclear cell.

No magnetic scattering was observed coinciding with nuclear scattering; the magnetic scattering obeyed both the condition $l' = 2n + 1$ and the rhombohedral condition $-h' + k' + l' = 3n$. It follows immediately that each magnetic moment has parallel partners at $\pm(\frac{2}{3}, \frac{1}{3}, \frac{1}{3})$ and antiparallel partners at $(0, 0, \frac{1}{2})$ and at $\pm(\frac{2}{3}, \frac{1}{3}, \frac{5}{6})$,

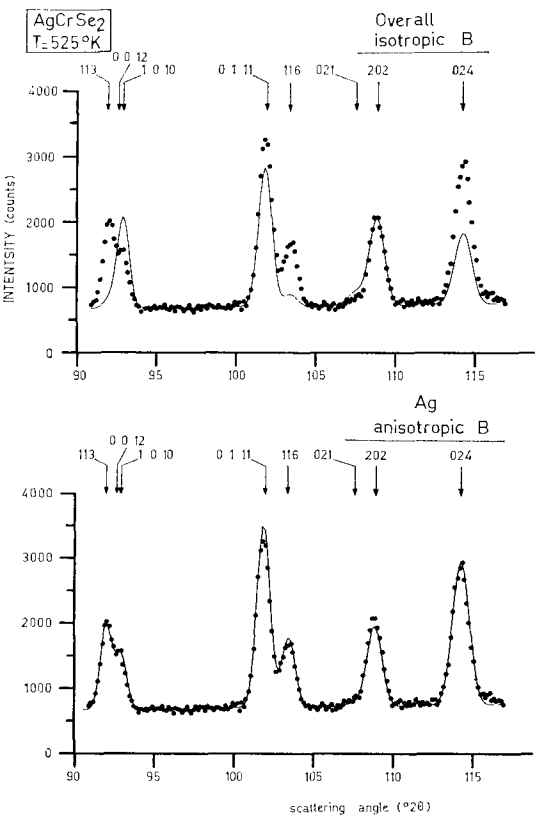

FIG. 3. Part of the neutron diffractogram of $AgCrSe_2$ at 525 K. The dots are the observed data. The line profiles (drawn curves) are calculated with an overall isotypic temperature factor (upper curve) and with the temperature factors given in Table IV (lower curve).

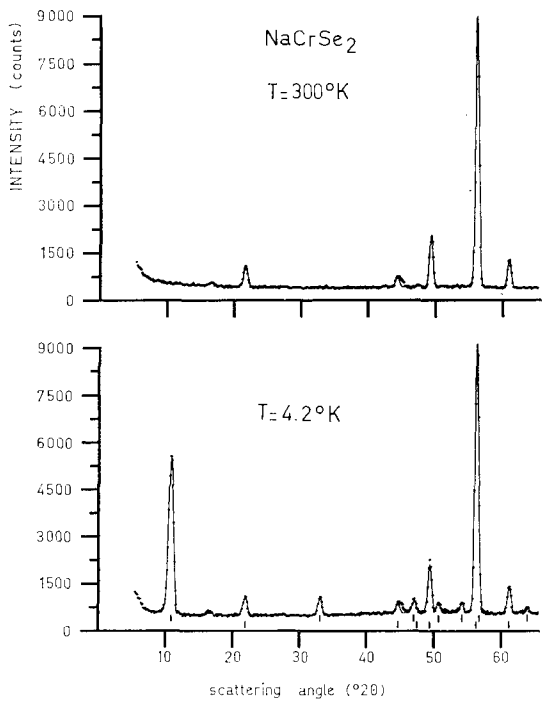

FIG. 4. Low-angle part of neutron diffractograms of $NaCrSe_2$ at 300 K and 4.2 K; observed data are given by dots, calculated line profiles by drawn curves.

in the magnetic unit cell, in agreement with the structure postulated by Bongers et al. (*1*); in the nuclear-cell description, moments at a distance $(\frac{1}{3},-\frac{1}{3},\frac{2}{3})$ are parallel, moments at a distance $(-\frac{1}{3},\frac{1}{3},\frac{1}{3})$ antiparallel.

An inspection of the intensities showed that the direction of the Cr^{3+} moments is perpendicular to the *c* axis; the direction of the spins in the basal plane cannot be determined because from powder data only values for the intensities averaged over equivalent reflections can be obtained. The final positional and magnetic parameters are given in Tables III and IV. Observed and calculated line profile data are shown in Fig. 4.

$AgCrSe_2$ and $NaCrS_2$

The neutron diagram of $AgCrSe_2$ at 4.2 K resembled at first sight that of $NaCrSe_2$ very closely. In a first attempt this diagram had been interpreted in a way analogous to that described for $NaCrSe_2$ in the preceding section, i.e., in terms of a model with ferromagnetic layers, coupled antiferromagnetically. However, in the case of $NaCrSe_2$ the fit of observed and calculated profiles was much better than in the case of $AgCrSe_2$. The difference between observation and calculation was especially striking for the first magnetic line, the position of which had been observed at an angle 2Θ about 0.2° higher than calculated on the basis of the $NaCrSe_2$ model (Fig. 5). Collecting new experimental data from the same sample led to an identical result. Furthermore a number of weak but nonzero peaks were not explained by this model. It was impossible to remove the above-mentioned difference of 0.2° by an indexing based on some multiple of the unit cell. Thus, the conclusion that in this case the structure is a modulated one seemed justified.

It turned out to be impossible to index the magnetic lines as satellites of nuclear reflections

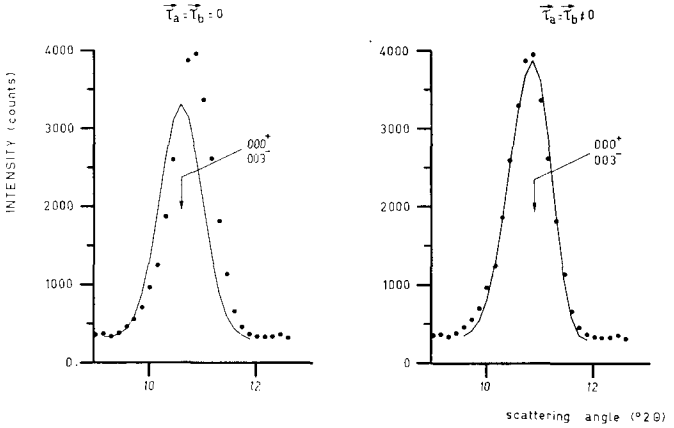

FIG. 5. First magnetic neutron-diffraction line of $AgCrSe_2$ at 4.2 K. The dots are the observed data. The line profile (drawn curve) on the left is calculated on basis of the $NaCrSe_2$ model ($\tau_c/c^* = \frac{3}{2}$; $\tau_a = \tau_b = 0$), the line profile on the right on basis of a helical model ($\tau_c/c^* = \frac{3}{2}$; $\tau_a = \tau_b \neq 0$).

assuming a propagation vector parallel or perpendicular to the c^* axis. A satisfactory agreement between observed and calculated peak positions was obtained with a propagation vector τ, which has components τ_a, τ_b, and τ_c along all three directions in reciprocal space. The fact that the first magnetic peak is single can be accounted for by the condition $\tau_c/c^* = \frac{3}{2}$, because this leads to equal 2Θ values for the peaks $(000)^+$ and $(003)^-$. τ_a and τ_b are relatively small and it is practically impossible to determine both components independently to a reasonable degree of accuracy. During the process of indexing, it became apparent that both components are equal in magnitude within the limits of the observation; therefore, the condition $|\tau_a| = |\tau_b|$ was adopted. Under this constraint the magnitude of the component was determined. The values for τ_a/a^* and τ_c/c^*, experimentally found are listed in Table V in both the hexagonal and the rhombohedral description which are related according to:

$$\begin{pmatrix} \tau_a/a^* \\ \tau_b/b^* \\ \tau_c/c^* \end{pmatrix}_{\text{rhomb}} = \begin{pmatrix} \frac{2}{3} & \frac{1}{3} & \frac{1}{3} \\ -\frac{1}{3} & \frac{1}{3} & \frac{1}{3} \\ -\frac{1}{3} & -\frac{2}{3} & \frac{1}{3} \end{pmatrix} \begin{pmatrix} \tau_a/a^* \\ \tau_b/b^* \\ \tau_c/c^* \end{pmatrix}_{\text{hex}}$$

The $NaCrS_2$ diagram at 4.2 K was indexed in an analogous way. Also in this case $\tau_c/c^* = \frac{3}{2}$.

The difference with $AgCrSe_2$ is that the a–b component of τ is about twice as large. As a result it is not possible to index the $NaCrS_2$ diagram even roughly on the $NaCrSe_2$ model.

In both $AgCrSe_2$ and $NaCrS_2$ only satellites of nuclear reciprocal lattice points that fulfil the rhombohedral condition $-h + k + l = 3n$ are present. This means that the relation between direction and magnitude of all Cr moments is governed by the propagation vector only. This simplifies the problem considerably. It only remains to decide whether the ordering scheme is either a helical structure or a modulated-amplitude type of structure. The scattering cross sections for these two ordering schemes are:

(i) For a helical structure:

$$\sigma_{\mathbf{H}\pm\tau} = \tfrac{1}{4}(1 + \cos^2\omega)\,[0.2695\mu_{\text{Cr}} f_{\text{Cr}}(\mathbf{H} \pm \tau)]^2,$$

where

ω is the angle between the axis of the helix and the scattering vector;

μ_{Cr} is the magnetic moment in Bohr magnetons of the Cr atom;

$f_{\text{Cr}}(\mathbf{H} \pm \tau)$ is the form factor of the Cr moment.

(ii) For a modulated-amplitude type of structure:

$$\sigma_{\mathbf{H}\pm\tau} = \tfrac{1}{4}\sin^2\omega\,[0.2695\mu^0_{\text{Cr}} f_{\text{Cr}}(\mathbf{H} \pm \tau)]^2,$$

where

ω is the angle between the spin direction and the scattering vector;

μ^0_{Cr} is the amplitude of the sinusoidal variation of the Cr moment.

It is seen that for a helical structure the cross section for magnetic scattering cannot vary by more than a factor of two for different reflections (apart from the variation of the form factor), while for a modulated-amplitude type of structure it can vary from zero to $\frac{1}{4}[0.2695\mu^0_{\text{Cr}} f_{\text{Cr}}(\mathbf{H} \pm \tau)]^2$.

In powder diagrams of rhombohedral compounds, reflections with different values of ω coincide in a systematic way, and only their average cross section can be observed. In general, it is still possible to distinguish the two structure models, but in the special case that $\tau // \mathbf{c}^*$ and the moments are perpendicular to the c axis, the two models are indistinguishable from powder data (*9*). In this case the average cross section for the two structure models becomes:

(i) $\langle\sigma_{\mathbf{H}\pm\tau}\rangle = \tfrac{1}{4}(1 + \cos^2\eta)\,[0.2695\mu_{\text{Cr}} f_{\text{Cr}}(\mathbf{H} + \tau)]^2$

(ii) $\langle\sigma_{\mathbf{H}\pm\tau}\rangle = \tfrac{1}{8}(1 + \cos^2\eta)\,[0.2695\mu^0_{\text{Cr}} f_{\text{Cr}}(\mathbf{H} + \tau)]^2;$

TABLE V

PROPAGATION VECTORS τ AND PERIODICITIES OF THE MAGNETIC STRUCTURES OF $NaCrSe_2$, $AgCrSe_2$, AND $NaCrS_2$ AT 4.2 K[a]

	$NaCrSe_2$	$AgCrSe_2$	$NaCrS_2$
Hexagonal			
τ_a/a^*	0	0.038(2)	0.092(1)
$\tau//b^*$	0	0.038(2)	0.092(1)
τ_c/c^*	$\frac{3}{2}$	$\frac{3}{2}$	$\frac{3}{2}$
Rhombohedral			
τ_a/a^*	$\frac{1}{2}$	0.538(2)	0.592(1)
$\tau//b^*$	$\frac{1}{2}$	$\frac{1}{2}$	$\frac{1}{2}$
τ_c/c^*	$\frac{1}{2}$	0.462(2)	0.408(1)
$\lvert\tau\rvert^{-1}$ (Å)	13.492(3)	13.47(2)	10.73(7)
$<(\tau, \mathbf{c}_{\text{hex}})$	0°	16 (3)°	33 (7)°
$\mu(\mu_B)$	2.63(3)	2.55(3)	2.48(4)
$<(\mu, \mathbf{c}_{\text{hex}})$	90°	90°	90°

[a] τ_a, τ_b, and τ_c are the components of τ along $\mathbf{a}^*$, $\mathbf{b}^*$, and $\mathbf{c}^*$. The magnetic moments derived by neutron diffraction are also given.

in both models, η is the angle between the hexagonal c^* axis and the scattering vector.

In $AgCrSe_2$ and $NaCrS_2$, the moments are indeed perpendicular to c, while the angle between $\boldsymbol{\tau}$ and $\mathbf{c}^*$ is rather small (Table V). For $AgCrSe_2$ the line profiles calculated for the two models are not significantly different, while in the case of $NaCrS_2$ the helical model gives a somewhat better fit for some small peaks.

For physical reasons a modulated-amplitude type of ordering of the Cr moments is most unlikely. The experimental evidence reported by Bongers et al. (*1*) also favors the existence of a helical ordering in $NaCrS_2$. Therefore, a helical ordering scheme is adopted for $NaCrS_2$ and, because of the resemblance of the diagrams of $NaCrS_2$ and $AgCrSe_2$, also for the latter compound.

In the helical ordering scheme the magnetic moment at a position x, y, z is given by:

$$\mathbf{S}_{x,y,z} = \mu_{Cr}\{\hat{x}\cos 2\pi[(\tau_a/a^*)x + (\tau_b/b^*)y + (\tau_c/c^*)z + \Phi_0] + \hat{y}\sin 2\pi[(\tau_a/a^*)x + (\tau_b/b^*)y + (\tau_c/c^*)z + \Phi_0]\},$$

where $\hat{x}$ and $\hat{y}$ are orthogonal unit vectors in the basal plane and Φ_0 is the phase angle of the moment at 0, 0, 0. The plane of the helix is assumed to be the basal plane as follows from the final calculations.

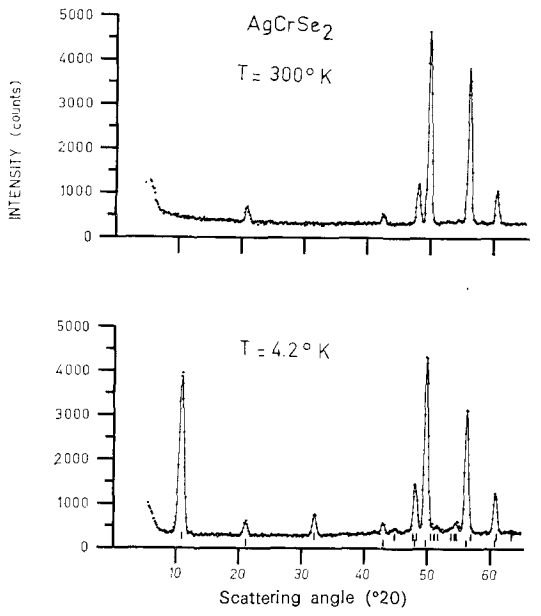

FIG. 6. Low-angle part of neutron diffractograms of $AgCrSe_2$ at 300 K and 4.2 K; observed data are given by dots, calculated line profiles by drawn curves.

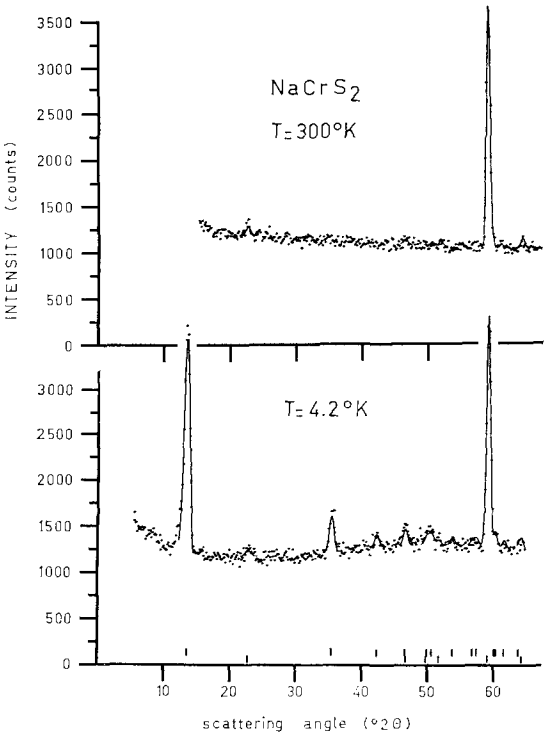

FIG. 7. Low-angle part of neutron diffractograms of $NaCrS_2$ at 300 K and 4.2 K; observed data are given by dots, calculated line profiles by drawn curves.

Final values of the parameters are listed in Tables III and V; observed and calculated line profiles are given in Figs. 6 and 7.

Again the apparent thermal motion of Ag^+ in $AgCrSe_2$ is anisotropic; it corresponds to an rms deviation $\mu_a = 0.2$ Å.

6. Discussion of the Magnetic Structures

The magnetic ordering schemes of $NaCrSe_2$, $AgCrSe_2$, and $NaCrS_2$ can be considered as helimagnetic. The moments in pseudohexagonal (110) planes (but not in $(\bar{2}10)$ or $(1\bar{2}0)$ planes) are collinear, spins at a distance $(-\frac{1}{3},\frac{1}{3},\frac{1}{3})$ being antiparallel, spins at a distance $(\frac{1}{3},-\frac{1}{3},\frac{2}{3})$ parallel (Fig. 8). The spins in adjacent (110) planes make angles φ, where $\varphi = 0°$ for $NaCrSe_2$, $\varphi = 14°$ for $AgCrSe_2$, and $\varphi = 33°$ for $NaCrS_2$. Thus, the modulation period in the hexagonal layers is infinite, 47.4 Å, and 19.4 Å, respectively, at 4 K. In $NaCrSe_2$ all spins in a layer are parallel, while in $AgCrSe_2$ and $NaCrS_2$ the spin at a certain Cr atom makes angles of $+\varphi, +2\varphi, +\varphi, -\varphi, -2\varphi$, and $-\varphi$ with the spins on its six nearest Cr neighbors (Fig. 9).

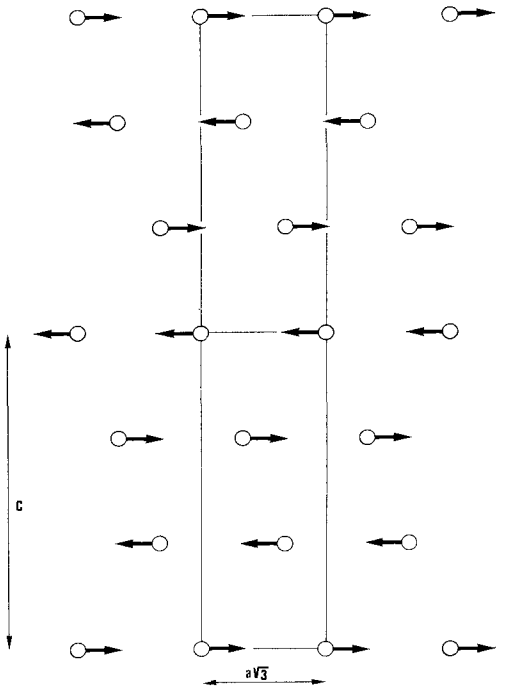

FIG. 8. Magnetic structures of $NaCrSe_2$, $AgCrSe_2$, and $NaCrS_2$; section through the (pseudo)hexagonal (110) planes.

The compound $KCrS_2$ is isostructural with $NaCrSe_2$, and it has the same magnetic structure at 4 K (*10*). The crystal structure of $LiCrS_2$ is somewhat different, the sulfur atoms forming a hexagonal rather than a cubic close-packing (*11*). However, the arrangement of the magnetic moments in the hexagonal planes of $LiCrS_2$ may be described in the same way as for the other compounds under discussion, φ being 120° for $LiCrS_2$ (Fig. 9).

There is a close correlation between the Cr–Cr distances within the hexagonal layers (equal to the cell edge *a*), the asymptotic Curie temperatures Θ, and the angles φ (Table VI). This correlation can be understood by considering the interactions between the spins of adjacent Cr^{3+} ions (*12*). This interaction is in part due to direct cation–cation exchange across the common edges of adjacent CrX_6 (X = S, Se) octahedra, involving the t_{2g} orbitals of the two cations. In Cr^{3+} the t_{2g} orbitals are half filled, favoring antiferromagnetic coupling of the spins. The cation–anion–cation interaction must also be considered. As the angle Cr–X–Cr is close to 90°, this interaction mainly involves *p* orbitals of the anion, a t_{2g} orbital (half filled) of one of the

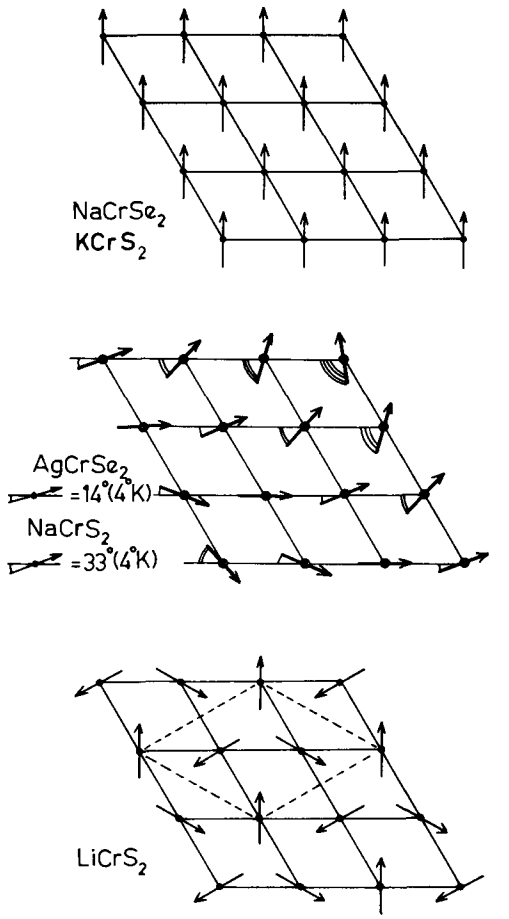

FIG. 9. Basal planes of the magnetic structures of $NaCrSe_2$ and $KCrS_2$ (upper figure); $AgCrSe_2$ and $NaCrS_2$ (middle figure); $LiCrS_2$ (lower figure).

TABLE VI

SHORTEST Cr–Cr DISTANCES *a*, ASYMPTOTIC CURIE TEMPERATURES Θ, AND ANGLES φ ($= 360° \cdot \tau_a/a^*$) FOR THE COMPOUNDS $ACrX_2$[a]

	a (4.2 K)	Θ	φ (4.2 K)
$KCrS_2$ (*10*)	3.601 Å	+112 K	0°
$NaCrS_2$	3.556	+30	33°
$AgCrS_2$	3.488	−55	
$CuCrS_2$	3.473	−90	
$LiCrS_2$ (*11*)	3.451	−276	120°
$NaCrSe_2$	3.732	+108	0°
$AgCrSe_2$	3.690	+72	14°

[a] A = Li, Na, K, Cu, Ag; X = S, Se.

cations, and an e_g orbital (empty) of the other cation; therefore, this interaction favours ferromagnetic coupling of the spins.

Direct cation–cation exchange is much more sensitive to the cation–cation distance than is the exchange via the anions. It is, therefore, expected that direct Cr^{3+}–Cr^{3+} exchange predominates for short Cr–Cr distances, exchange via the anions for large Cr–Cr distances leading to a ferromagnetic arrangement of the moments within a layer, in complete agreement with the observations.

The interactions between the moments in different layers cannot easily be discussed in terms of this simple model. Since these interactions must involve at least two anions, they are expected to be much weaker than the intralayer coupling of the spins, in agreement with observation (*1*). Therefore, the asymptotic Curie temperatures will mainly be determined by the intralayer interactions.

It is tempting to speculate from the data in Table VI that $AgCrS_2$ and $CuCrS_2$ would have magnetic structures with φ between 60° and 120°. Actually, the magnetic structures of $AgCrS_2$ and $CuCrS_2$ are more complex than those of the other compounds; their determination is in progress. It should finally be emphasized that the ordering scheme determined for $NaCrS_2$ is different from that assumed by Bongers et al. (*1*) and by Carr et al. (*13*) to explain their magnetization and NMR data, respectively; the latter model consisted of a helix with all spins in a layer parallel and propagating along **c***.

References

1. P. F. Bongers, C. F. van Bruggen, J. Koopstra, W. P. F. A. M. Omloo, G. A. Wiegers, and F. Jellinek, *J. Phys. Chem. Solids* **29**, 977 (1968).
2. R. de Jonge, T. J. A. Popma, G. A. Wiegers, and F. Jellinek, *J. Solid State Chem.* **2**, 188 (1970).
3. B. O. Loopstra, *Nucl. Instrum. Methods* **44**, 181 (1966).
4. H. M. Rietveld, *J. Appl. Crystallogr.* **2**, 65 (1969).
5. R. F. Watson and A. J. Freeman, *Acta Crystallogr.* **14**, 27 (1961).
6. J. W. Boon and C. H. MacGillavry, *Rec. Trav. Chim. Pays-Bas* **61**, 910 (1942).
7. W. Rüdorff and K. Stegemann, *Z. Anorg. Allg. Chem.* **251**, 376 (1943).
8. W. Rüdorff, W. R. Ruston, and A. Scherhaufer, *Acta Crystallogr.* **1**, 196 (1948).
9. G. Shirane, *Acta Crystallogr.* **12**, 282 (1959).
10. B. van Laar and F. M. R. Engelsman, *J. Solid State Chem.*, in press.
11. B. van Laar and D. J. W. IJdo, *J. Solid State Chem.* **3**, 590 (1971).
12. J. B. Goodenough, "Magnetism and the Chemical Bond," Interscience, New York–London (1963).
13. S. L. Carr, P. Erdös, W. G. Moulton, and J. Robinson, *Solid State Commun.* 7, 1673 (1969).